Proc. Natl. Acad. Sci. USA
Vol. 87, pp. 1–5, January 1990
Biophysics

Temperature-derivative spectroscopy: A tool for protein dynamics

(nonisothermal relaxation/myoglobin/substates/enthalpy distributions/flash photolysis)

JOEL BERENDZEN* AND DAVID BRAUNSTEIN†

Departments of *Biophysics and †Physics, University of Illinois at Urbana–Champaign, 1110 West Green Street, Urbana, IL 61801

Communicated by Hans Frauenfelder, October 6, 1989 (received for review July 10, 1989)

ABSTRACT **A relaxation method that measures the derivative of a population with respect to temperature is introduced and used to study the recombination of CO to sperm whale myoglobin after a photolyzing flash. Measurement of the geminate process in the infrared CO-stretch bands shows distributed activation enthalpies with different distributions for each band, transitions between two bands that correspond to photolyzed ligands, and kinetic hole burning. The data are well described by gaussian enthalpy distributions; the results match and complement those of isothermal methods. The temperature-derivative technique is further used to explore the recombination of CO from outside the heme pocket.**

Flexibility and motion are essential to protein function (1–3); relaxation experiments provide a powerful means for their study (4). Starting with an ensemble of proteins in equilibrium, one introduces a perturbation [a flash of light or a change in pressure, for example (5, 6)] and records the response of the observable (typically a spectroscopic marker such as light absorption) as the proteins relax toward a new equilibrium. Analysis of the time and temperature dependence of the response yields information about motions and reactions. Synthesis of results from many such experiments that use different observables and perturbations leads to a "global" picture of the protein from which new understanding may emerge.

Distributed rates are a nearly universal feature of protein ensembles at low temperature. That is, their responses may be described by sums of exponential terms with rates so closely spaced as to form a continuum. These rate distributions, which can cover many orders of magnitude, arise from conformational differences among proteins (5, 7).

In isothermal relaxation spectroscopy (IRS), the relaxation technique most commonly used for protein dynamics, the temperature is held constant after the perturbation, as shown in Fig. 1*A*. Unfortunately, IRS can be taxing when applied to systems with widely distributed rates, for no single time scale will be appropriate at a given temperature; even specially designed instruments using logarithmic time base digitizers (8, 9) cannot cover rates spanning more than about 12 decades. So, data are collected over the widest practical time range and are analyzed by applying a model that combines results from several different temperatures to describe distributions in activation enthalpy or entropy or both.

As an alternative to isothermal relaxation measurements, we have monitored changes in an observable with time under nonisothermal conditions, as shown in Fig. 1*B*. The temperature was ramped from an initial value T_i at a rate β, such that

$$T = T_i + \beta t. \qquad [1]$$

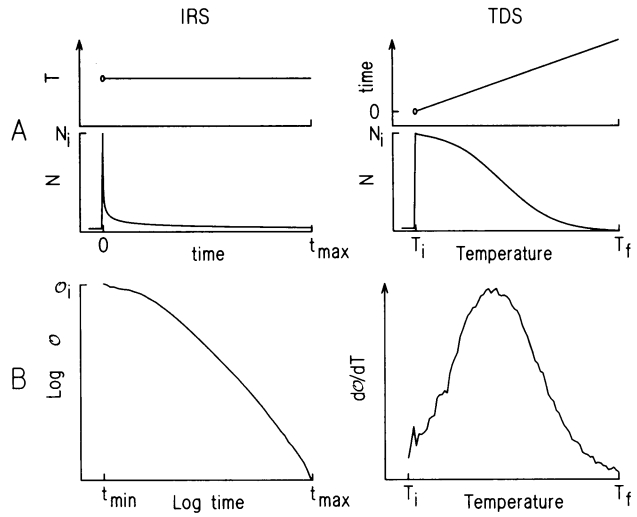

FIG. 1. IRS and TDS. (*A*) An initial perturbed population N_i is created at time $t = 0$ and its relaxation is measured. In IRS, the temperature is fixed at a value where the rates are convenient to measure. In TDS, the temperature is linearly ramped and relaxation proceeds as rates increase with increasing temperature. (*B*) In IRS, one measures the decay of the observable over the broadest possible range in time. In TDS, one measures changes in the observable between sequential measurements from a temperature low enough so that the rates are extremely slow to one high enough so that the population is depleted.

Assuming the observable, $\mathcal{O}$, is proportional to an out-of-equilibrium population N plus a constant (the "baseline"), the change in $\mathcal{O}$ per time interval Δt is then

$$\lim_{\Delta t \to 0} \frac{\mathcal{O}(t + \Delta t) - \mathcal{O}(t)}{\Delta t} = \frac{d\mathcal{O}}{dt} = c\beta \frac{dN}{dT}, \qquad [2]$$

where c is a constant.‡ The change in the observable with time is thus directly proportional to the temperature derivative of the population, dN/dT, which for a given model can be related to parameters such as activation enthalpy and entropy.

A crude understanding of such measurements on rate processes may be achieved without a specific model: dN/dT will be small at low temperatures where rates are low, but will increase as the rates increase with increasing temperature. At high temperatures, dN/dT is again small because the population N has been depleted. The signal thus peaks at some intermediate temperature, T_p, that is determined by the

The publication costs of this article were defrayed in part by page charge payment. This article must therefore be hereby marked "*advertisement*" in accordance with 18 U.S.C. §1734 solely to indicate this fact.

Abbreviations: IRS, isothermal relaxation spectroscopy; TDS, temperature-derivative spectroscopy.

‡Eq. 2 implicitly assumes that c is independent of temperature and that only the population N contributes to changes in the observable; subtraction or scaling may be used to correct for deviations from these assumptions.

heating rate and the barrier parameters—the higher the barriers, the higher the peak temperature.

Nonisothermal relaxation experiments have been used to study a variety of phenomena: the resistance of thin metal films (tempering) (10), the emission of light and electrons from solids after irradiation (thermoluminescence and exoemission) (11), and the electrical response of insulators and semiconductors to applied fields (thermally stimulated current and capacitance) (12, 13). These experiments share a mathematical framework; we call them examples of temperature-derivative spectroscopy (TDS).

We reinvented TDS during studies of the rebinding of CO to the protein myoglobin (Mb) after a photolyzing flash. We chose to monitor the reaction in the infrared CO-stretch absorption bands, because they are rich in spectroscopic information that can be correlated with structural and dynamic properties of the protein. The region from 1890 to 2000 cm^{-1} in heme proteins contains absorption bands from substates of CO bound to the heme (A substates), while the region from 2100 to 2200 cm^{-1} contains weaker bands from photolyzed ligands that remain in the heme pocket (B substates) (14–16). In native sperm whale Mb, there are at least three A substates and three B substates; a summary of their characteristics is presented in Table 1.

Table 1. Properties of the infrared CO-stretch bands of sperm whale MbCO at 10 K and pH 7

Substate	Fraction	ν_p, cm^{-1}	α,°*
A_0	0.1	1966	15 ± 10
A_1	0.8	1945	28 ± 2
A_3	0.1	1927	33 ± 4
B_0	0.1	2149	NA
B_1	0.7	2130	NA
B_2	0.2	2119	NA

ν_p, Peak wavenumber of the band; α, angle between the heme normal and the C—O bond; NA, not applicable, since α is random for CO in the B (pocket) substates.
*From ref. 17.

Methods and Data

A 20 mM solution of sperm whale Mb from lyophilized powder (Sigma) was prepared in 75% glycerol/25% water (vol/vol) buffered to pH 6.9 at room temperature with 0.1 M potassium phosphate. Sodium dithionite in 4-fold excess was used to reduce the protein solution, which was then saturated with CO. A few microliters of this solution, held between CaF_2 windows spaced 125 μm apart with a mylar washer, yielded a red spot of 5 mm diameter with an absorbance of 0.4 at the peak of the dominant A_1 stretch band.

The CaF_2 windows were then sandwiched inside a 1.5 × 2.5 × 4 cm^3 piece of oxygen-free high-conductivity copper to which a Si temperature-sensor diode was attached; the whole assembly was mounted on a He refrigerator (Cryosystems 22C, Tucson, AZ). A programmable digital temperature controller (Lakeshore Cryotronics DRC93, Westerville, OH) enabled this design to obtain linear heating rates from 1 to 25 mK/s over the range 12–350 K.

The sample was cooled in the dark to 12 K and then photolyzed with 20 s of 514.5-nm light from an Ar^+ laser (Spectra-Physics 164, Mountain View, CA) operating at an intensity of 0.5 W/cm^2. The temperature increase of the sample during photolysis was <1 K. Spectra were taken repetitively at 2 cm^{-1} resolution on a Fourier transform IR spectrophotometer (Mattson Sirius 100, Madison, WI). An 800 cm^{-1} HgCdTe detector was used. Spectra were collected for 210 s each, with 30 s allowed for computation between measurements. Successive absorbance spectra were subtracted from each other and divided by $\beta\Delta t$ to produce temperature-derivative signals of dA/dT vs. temperature and wavenumber.

Fig. 2 shows data from a single 10-hr TDS experiment, taken at a heating rate of 3.125 mK/s after photolysis at 12 K. The reappearance of the A substates generates positive signals, while the disappearance of the B substates generates negative signals. Qualitative features of the data immediately corroborate the results of previous work: (*i*) Recombination occurs over wide ranges in temperature, pointing to a distribution in activation enthalpies (5). (*ii*) The TDS signals appear as broad peaks without sharp features, implying that the enthalpy distribution must be similarly smooth (18). Numerical simulations have shown that at least 70 discrete

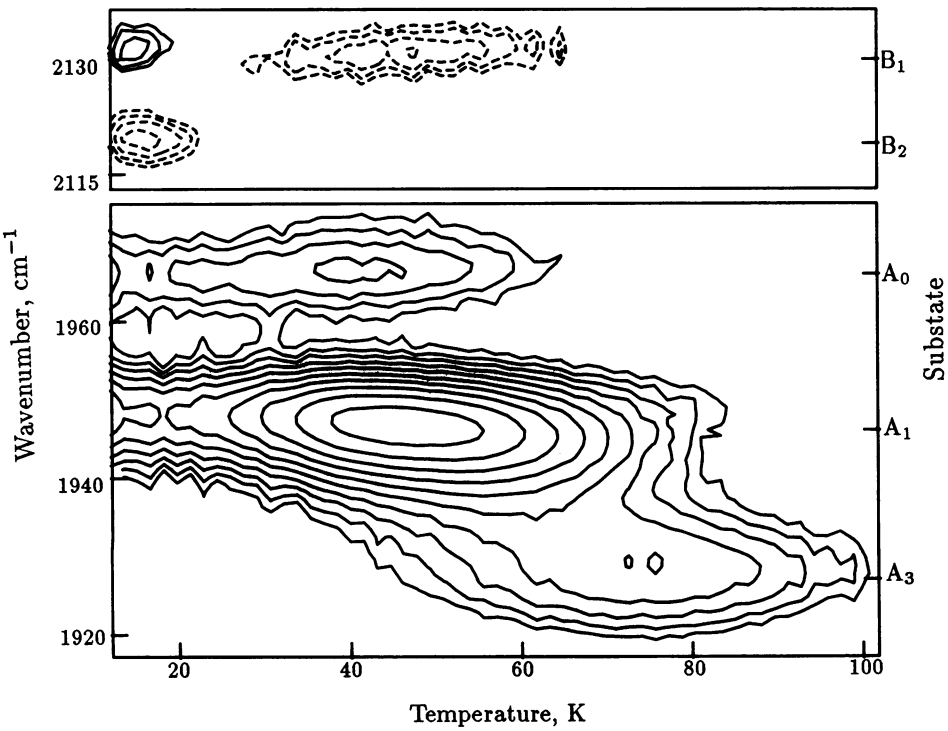

FIG. 2. IR–TDS data obtained on warming sperm whale MbCO after a photolyzing flash at 12 K, as monitored in the A (bound) and B (pocket) CO-stretch bands. Data are presented as contours of dA/dT, spaced logarithmically for added contrast, with six contours per decade above the lowest contour level of $\pm 0.32 \times 10^{-3}$ OD/K. Positive contour levels are drawn as solid lines and negative contour levels are drawn as dashed lines. Because the B substates have extinction coefficients that are more than a factor of 10 smaller than those of the A substates, less of the B_1 and B_2 TDS signals are above the lowest contour level and B_0 is entirely within the noise.

enthalpy values in each of the substates would be required to achieve the degree of smoothness displayed in Fig. 2. (*iii*) The Gibbs free energy barrier to recombination from inside the pocket is higher for A_3 than it is for A_0 and A_1, since the A_3 TDS signal peaks at a higher temperature (18). (*iv*) The state B_1 grows at the expense of B_2 below 30 K, a process also governed by a distributed enthalpy barrier (14). (*v*) Contours of dA/dT for substates A_0 and B_1 shift to higher wavenumbers with increasing temperature; those for A_1 shift to lower wavenumbers. Stated another way, the high- and low-wavenumber sides of the substate marker bands have different barrier heights. These effects are known as kinetic hole burning and point to a further level of inhomogeneity within each substate (19–21).

First-Order Rate Processes

Changes in the population N may arise not only from rate processes, but also from exchange among populations as equilibria shift with temperature. The two are readily distinguishable because reversing the direction of the temperature scan will reverse exchange but not rate processes. We shall consider only the nonequilibrium case, since TDS offers little advantage over traditional methods for studying time-independent phenomena. In this section, we develop a quantitative model for low-temperature ligand rebinding, based on first-order rates with Arrhenius temperature dependence and distributed enthalpies.

First-order (or pseudo-first-order) rate processes are ubiquitous and their mathematics in this context has been described many times (11, 22). Starting from the definition of a first-order process,

$$\frac{dN}{dt} = -kN, \qquad [3]$$

where k is the rate coefficient, one applies the experimental constraint, Eq. **1**, and integrates to obtain

$$\frac{dN}{dT} = \frac{-N_i}{\beta} k e^{-\Theta}, \qquad [4]$$

where

$$\Theta = \int_{T_i}^{T} \frac{k}{\beta}\, dT', \qquad [5]$$

and N_i is the initial population of the perturbed state.

We shall take rates to be given by the Arrhenius relation with a temperature-dependent preexponential factor:

$$k = A\left(\frac{T}{T_r}\right)^n e^{-H/RT}, \qquad [6]$$

where A is the preexponential at the arbitrary reference temperature T_r, n is an integer between -2 and 2, H is the enthalpic barrier, and R is the gas constant. Eq. **5** may then be recast as

$$\Theta = \frac{AT_r}{\beta}\left[\left(\frac{T}{T_r}\right)^{n+1} E_{n+2}\left(\frac{H}{RT}\right) - \left(\frac{T_i}{T_r}\right)^{n+1} E_{n+2}\left(\frac{H}{RT_i}\right)\right], \qquad [7]$$

where

$$E_m(x) = \int_1^\infty \frac{e^{-xt}}{t^m}\, dt \qquad [8]$$

is the exponential integral of order m, a function that may be evaluated by a variety of numerical techniques (24–26).

Evaluation of Eqs. **4–8** yields the intrinsic line shape for TDS. The width of this line shape, which depends on enthalpy, preexponential, and heating rate, is one limit to the energy resolution of the experiment. For example, taking $H = 10\,\text{kJ/mol}$, $A = 10^9\,\text{s}^{-1}$, $T_r = 100\,\text{K}$, $n = 1$, $\beta = 3.125\,\text{mK/s}$, and $T_i = 12\,\text{K}$ (values typical of those in Fig. 2), dN/dT would be sharply peaked at 46 K with a full width at half maximum of 4 K. Increasing the enthalpy while holding the preexponential fixed causes the width to increase approximately linearly with the peak temperature, T_p (27).

The relation between T_p and H may be further clarified by taking the second derivative of N with respect to time and setting it equal to zero. Eq. **3** then yields $k = k^2$, which for Arrhenius rates implies that

$$T_p = \frac{H}{R \ln(A\tau_c)}, \qquad [9]$$

where

$$\tau_c = \frac{RT_p^2}{\beta(H + nRT_p)}\left(\frac{T_p}{T_r}\right)^n \qquad [10]$$

is the characteristic time for a TDS measurement (28). Thus, for a given preexponential, the relation between H and T_p is nearly linear, since $\ln(A\tau_c)$ varies slowly with T_p. For parameters in the range of those discussed above, the relation is given crudely by $H \approx 25RT_p$.

We now introduce an enthalpy distribution, in which each protein reacts independently, with a unique activation enthalpy H. To describe the behavior of an ensemble of such proteins, one sums Eq. **4** (which describes the behavior of proteins with a single activation enthalpy) over the range of enthalpies present, weighting each term by the number of proteins with that enthalpy. In the limit of a continuous enthalpy distribution, dN/dT is given by the integral

$$\frac{dN}{dT} = -\frac{N_i}{\beta}\int_0^\infty k e^{-\Theta} g(H)dH, \qquad [11]$$

where $g(H)dH$ is the probability of any protein having an activation enthalpy between H and $H + dH$, normalized to 1. We shall apply this equation to the interpretation of the data in Fig. 2.

It may be seen from the distributed enthalpy expression, Eq. **11**, that if the distribution is broad compared to the intrinsic linewidth and T_p goes linearly with H, then dN/dT vs. T will be crudely proportional to $g(H)$ vs. H. Proper calculation, though, of the shape and position of the enthalpy distribution requires knowledge of the preexponential. T_p (and thus the entire TDS curve) may be shifted slightly in temperature by varying the heating rate, and the amount of this shift can, in principle, give the preexponential factor. But, since $A/\tau_c >> 1$ for most realizable heating rates, the size of this shift may be too small to constrain the preexponential. A better approach may be to combine the results of TDS measurements with those of complementary IRS measurements, as suggested by Pender and Fleming (29).

Interpretation

In Fig. 3, we plot dA/dT vs. T at the 10 K absorption peaks of the A and B substates. The solid curves in Fig. 3 are least-squares fits to the data, generated by the model advanced in the previous section, with $g(H)$ given by gaussian enthalpy distributions truncated at $H = 0$. Excepting substates A_1 and A_0 below 25 K where tunneling is significant (30), this model describes the data well.

While careful IRS measurements in the Soret have been able to resolve gaussian-like substate enthalpy distributions (31), TDS affords their best description. Gaussian enthalpy distributions arise naturally from models in which the barrier

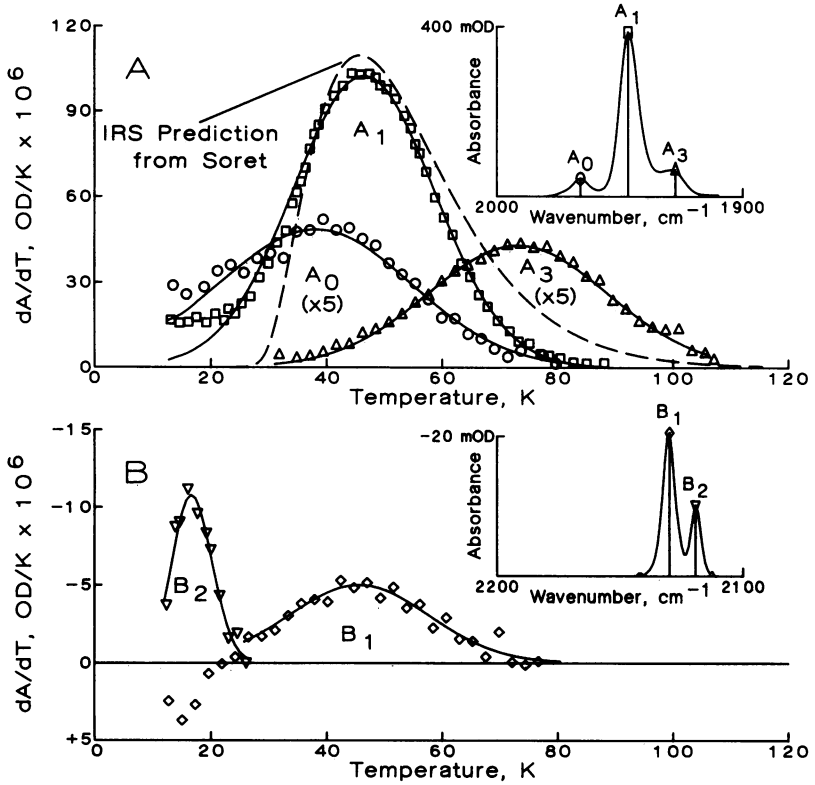

FIG. 3. TDS signals (symbols) and fits to gaussian distributions of activation enthalpies (lines) at the peaks of the A substates (*A*) and the B substates (*B*). (*Insets*) Difference spectra after photolysis at 12 K with symbols indicating the points at which the fits are made. The positive B_1 signal below 25 K is due to the process $B_2 \rightarrow B_1$.

is determined by the sum of many independent, identical contributions (32). Specific models predicting gaussian distributions for low-temperature ligand binding in heme proteins have been proposed by Agmon and Hopfield (33, 34) and by Stein (35).

Parameters of fits to IRS (15, 18) and TDS measurements are shown in Table 2. For the TDS fits, the preexponential values were taken from the infrared IRS results in column 4 of Table 2, with $n = 1$ and $T_r = 100$ K as for the IRS fits (23). These measurements represent the first determination of Γ for each A substate, so the values of Γ cannot be compared with published results. The H_p values agree well, except for those of A_1, which shows a small discrepancy. However, fits to IRS measurements in the Soret using a gamma-distributed enthalpy give $H_p = 10.1$ kJ/mol, $\Gamma = 6.6$ kJ/mol, and $A = 10^9$ s^{-1} for $n = 1$ and $T_r = 100$ K and predict the dashed line in Fig. 3*A* (18). This prediction agrees well with TDS data on the dominant A_1 population.

The fits to the B substates shown in Fig. 3*B* assume that direct recombination from B_2 is negligible and that the preexponential for B_1 recombination is identical to that for A_1. Although the values of H_p and Γ calculated for B_1 and A_1 agree, the question of the mapping between the A and B substates remains open, since any B-state TDS signal corresponding to A_3 is too small to be detected at this pH.

Table 2. Kinetic properties of sperm whale Mb at pH 6.9 as determined by IRS and TDS

Kinetic process	ν_p, cm^{-1}	IRS		TDS	
		H_p	log A	H_p	Γ
$B \rightarrow A_0$	1966	10*	10.8*	9.5	11
$B \rightarrow A_1$	1945	9.5*	9.3*	10.8	7.0
$B \rightarrow A_3$	1927	18*	9.8*	17.8	9.0
$B_1 \rightarrow A$	2130	—	—	10.4	7.0
$B_2 \rightarrow B_1$	2119	3.7†	11†	4.1	2

The preexponential values determined by IRS measurements were used for the TDS calculations. ν_p, Peak wavenumber at 10 K, at which the observation was made; H_p, peak of the enthalpy distribution in kJ/mol; A, preexponential at 100 K in s^{-1}; Γ, full width at half maximum of the enthalpy distribution in kJ/mol.
*From ref. 17.
†From ref. 14.

Further Applications

The biggest distinction between TDS measurements and standard time-resolved methods is one of measurement strategy. TDS measures changes over a single rate window at a variety of temperatures, while IRS determines a wide range of rates at a single temperature. Because of the restriction of TDS to time scales in which thermal equilibration is possible, a set of IRS measurements can, in principle, give more information about the dynamics of the system. However, TDS can complement isothermal methods with its own unique advantages: (*i*) Compared to similar IRS measurements over wide ranges in time and temperature, TDS measurements are easy to implement and run. (*ii*) For rate processes characterized by a distributed enthalpy at low temperatures, the signal is distributed nearly evenly across the entire range of energies present. Also, the measured quantity $\Delta\mathcal{O}$ is crudely proportional to the enthalpy distribution $g(H)$, which allows for quick interpretation of data in advance of computer fitting. (*iii*) TDS has no intrinsic restriction on the time resolution required of the spectrometer. The time scale for a TDS experiment is set by the heating rate and may be as slow or as fast as thermal equilibration times, instrumental stability, and patience permit. This flexibility not only permits determination of kinetic parameters from very slow instruments but also allows the use of slow perturbations.

An example of such a perturbation studied by TDS is shown in Fig. 4. The MbCO sample described above was cooled from 260 K to ≈160 K at a rate of 6.25 mK/s while photolyzing continuously with 514.5-nm light at 20 W/cm^2, giving a photolysis rate of ≈50 s^{-1}. In this manner, ≈10% of the proteins were held in a metastable state with no ligands in the pocket at 160 K. The photolysis beam was then switched off and the sample was allowed a few minutes to come to thermal equilibrium. The sample was next warmed

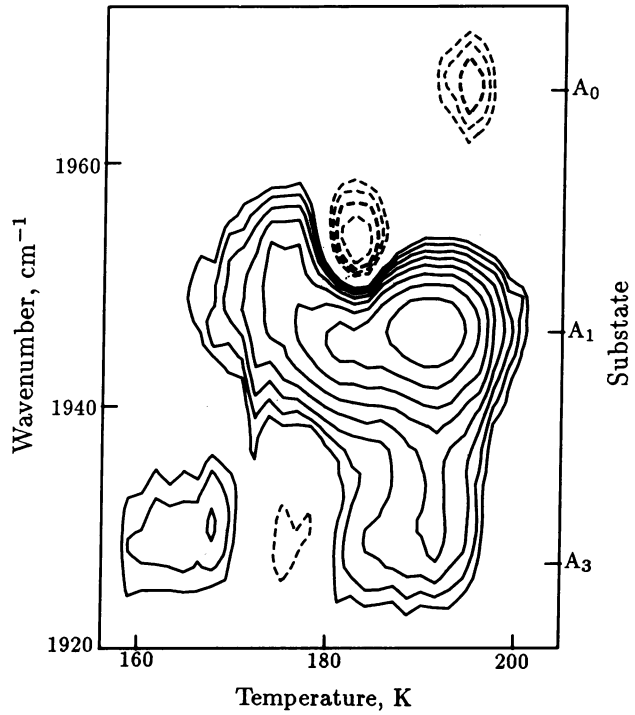

FIG. 4. TDS study of ligand recombination from outside the pocket. An out-of-equilibrium state was created by photolyzing continuously while cooling from 260 K to 160 K. The light was then switched off and the sample was warmed in the dark as the TDS signal was measured. A "background" TDS signal of equilibrium exchange has been subtracted from the data. Contour levels are as given in Fig. 2.

at a rate of 6.25 mK/s as the TDS signal was measured. A nontrivial equilibrium exchange among the A substates (the TDS signal recorded in the absence of photolysis) was subtracted from this signal.

A positive net signal was observed, corresponding to recombination of CO from outside the pocket, but the IR–TDS map is complicated. First, a significant fraction of the A_3 (but not A_1) population recombined at ≈165 K and underwent two spectroscopically distinguishable shifts as the sample was warmed to the solvent's glass-transition temperature (6). At the glass temperature, there was a large positive signal in both the A_1 and A_3 substates as ligands rebound. A negative signal, however, was observed for substate A_0 as the system equilibrated its substate populations.

From this result, it would appear that the barriers to recombination from outside the pocket may be quite different for the different substates. This is consistent with the notion that conversion between the substates involves a global rearrangement of the protein. Further analysis of this type of experiment should yield information about the rates of the recombination from outside the pocket and exchange among the substates.

Temperature-derivative spectroscopy is not a new technique, but it offers promise for studies in protein dynamics. It may be used with a variety of observables, such as circular dichroism, Raman scattering, and fluorescence anisotropy. The possibility of combining TDS with x-ray or neutron diffraction to yield detailed information about structural dynamics is particularly exciting. Its relative ease of implementation and interpretation make it an excellent survey technique, and it may also be used as a precise quantitative tool.

It is a pleasure to acknowledge the helpful advice and criticism of Ben Cowen, Prof. Enrico Gratton, J. Bruce Johnson, Stan Luck, Judith Mourant, Pál Ormos, Todd Sauke, Reinhard Scholl, Peter Steinbach, Prof. Robert D. Young, and Aihua Xie. J.B. would like to thank the late Prof. Ted Stoddard for his patient explanation of thermoluminescence. Special thanks are due to Prof. Hans Frauenfelder for his advice and support. This work was supported by Grant DMB82-09616 of the National Science Foundation and Grants GM18051 and GM32455 of the National Institutes of Health.

1. Careri, G., Fasella, P. & Gratton, E. (1979) *Annu. Rev. Biophys. Bioeng.* **8**, 69–97.
2. Frauenfelder, H., Parak, F. & Young, R. D. (1988) *Annu. Rev. Biophys. Biophys. Chem.* **17**, 451–489.
3. Brook, C. L., III, Karplus, M. & Pettitt, B. M. (1987) *Adv. Chem. Phys.* **71**.
4. Eigen, M. & DeMaeyer, L. (1974) in *Investigation of Rates and Mechanisms of Chemistry*, Hammes, G., ed. (Wiley, New York), 3rd Ed., Pt. 2, pp. 63–146.
5. Austin, R. H., Beeson, K. W., Eisenstein, L., Frauenfelder, H. & Gunsalus, I. C. (1975) *Biochemistry* **14**, 5355–5373.
6. Iben, I. E. T., Braunstein, D., Doster, W., Frauenfelder, H., Hong, M. K., Johnson, J. B., Luck, S., Ormos, P., Schulte, A., Steinbach, P. J., Xie, A. H. & Young, R. D. (1989) *Phys. Rev. Lett.* **62**, 1916–1919.
7. Alcala, J. R., Gratton, E. & Prendergast, F. G. (1987) *Biophys. J.* **51**, 597–604.
8. Austin, R. H., Beeson, K. W., Chan, S. S., Debrunner, P. G., Downing, R., Eisenstein, L., Frauenfelder, H. & Nordlund, T. M. (1976) *Rev. Sci. Instrum.* **47**, 445–447.
9. Berendzen, J., Frauenfelder, H., Sauke, T. & Scholl, R. (1989) *Bull. Am. Phys. Soc.* **34**, 880 (abstr.).
10. Vand, V. (1943) *Proc. Phys. Soc. (London) Sect. A* **55**, 222–246.
11. Randall, J. T. & Wilkins, M. H. F. (1945) *Proc. R. Soc. London Ser. A* **184**, 366–389.
12. Bräunlich, P. ed. (1979) *Thermally Stimulated Relaxation in Solids* (Springer, Berlin).
13. Celaschi, S. & Mascarenhas, S. (1977) *Biophys. J.* **20**, 273–278.
14. Alben, J. O., Beece, D., Bowne, S. F., Doster, W., Eisenstein, L., Frauenfelder, H., Good, D., McDonald, J. D., Marden, M. C., Moh, P. P., Reinisch, L., Reynolds, A. H., Shyamsunder, E. & Yue, K. T. (1982) *Proc. Natl. Acad. Sci. USA* **79**, 3744–3748.
15. Alben, J. O., Moh, P. P., Fiamingo, F. G. & Altschuld, R. A. (1981) *Proc. Natl. Acad. Sci. USA* **78**, 234–237.
16. Doster, W., Bowne, S. F., Frauenfelder, H., Reinisch, L. & Shyamsunder, E. (1987) *J. Mol. Biol.* **194**, 299–312.
17. Ormos, P., Braunstein, D., Frauenfelder, H., Hong, M. K., Lin, S.-L., Sauke, T. S. & Young, R. D. (1988) *Proc. Natl. Acad. Sci. USA* **85**, 8492–8496.
18. Ansari, A., Berendzen, J., Braunstein, D., Cowen, B. R., Frauenfelder, H., Hong, M. K., Iben, I. E. T., Johnson, J. B., Ormos, P., Sauke, T. B., Scholl, R., Schulte, A., Steinbach, P. J., Vittitow, J. & Young, R. D. (1987) *Biophys. Chem.* **26**, 337–355.
19. Campbell, B. F., Chance, M. R. & Friedman, J. M. (1987) *Science* **238**, 373–376.
20. Agmon, N. (1988) *Biochemistry* **27**, 3507–3511.
21. Ormos, P., Ansari, A., Braunstein, D., Cowen, B. R., Frauenfelder, H., Hong, M. K., Iben, I. E. T., Sauke, T. B., Steinbach, P. & Young, R. D. (1990) *Biophys. J.* **51**, in press.
22. Primak, W. (1955) *Phys. Rev.* **100**, 5227–5232.
23. Dlott, D. D., Frauenfelder, H., Langer, P., Roder, H. & DiIorio, E. (1983) *Proc. Natl. Acad. Sci. USA* **80**, 6239–6243.
24. Stegun, I. A. & Zucker, R. (1974) *J. Res. Natl. Bur. Stand. Sect. B* **788**.
25. Agrawal, R. K. (1987) *J. Therm. Anal.* **32**, 149–156.
26. Press, W. H. & Teukolsky, S. A. (1988) *Comput. Phys.* **2**, 88–89.
27. Chen, R. & Kirsh, Y. (1981) *Analysis of Thermally Stimulated Processes* (Pergamon, Oxford), pp. 161–163.
28. Chen, R. & Winer, S. A. A. (1970) *J. Appl. Phys.* **41**, 5227–5232.
29. Pender, L. F. & Fleming, R. J. (1977) *J. Phys. C* **10**, 1561–1570.
30. Frauenfelder, H. (1979) in *Tunneling in Biological Systems*, eds. Chance, B., DeVault, D. C., Frauenfelder, H., Marcus, R. A., Schrieffer, J. R. & Sutin, N. (Academic, New York), pp. 627–649.
31. Steinbach, P. J., Frauenfelder, H., Johnson, J. B. & Sauke, T. B. (1989) *Biophys. J.* **55**, 565a (abstr.).
32. Macdonald, J. R. (1987) *J. Appl. Phys.* **62**, R51–R62.
33. Agmon, N. & Hopfield, J. J. (1983) *J. Chem. Phys.* **78**, 6947–6959.
34. Agmon, N. & Hopfield, J. J. (1983) *J. Chem. Phys.* **79**, 2042–2053.
35. Stein, D. L. (1985) *Proc. Natl. Acad. Sci. USA* **82**, 3670–3672.